Chapter 3
Experimental work

3.1 Work plan

This chapter describes the experimental procedures followed in preparation of fatigue test specimens, surface treatments, its characterization, procedures followed for fatigue evaluation and post-fatigue characterization.
The experimental procedures followed are briefly summarized as under:

The entire experimental work was divided into three phases, namely a pre-fatigue test phase, the actual testing phase, & the post-fatigue test phase.

- ***Pre-fatigue test phase***
  - Preparation of fatigue test specimens
  - Surface treatments using chrome-plating, thermal spray and plasma nitriding techniques
  - Characterization of the untreated (herein after called as base material) as well as surface treated specimens by techniques such as microstructure examination using optical microscopy, thickness and hardness measurements of surface treated layer, Energy Dispersive X-Ray Spectroscopy (EDS), and X-ray diffraction (XRD), etc.
- ***Fatigue testing phase***
  - Fatigue testing of base material as well as surface treated specimens in rotating bending mode
- ***Post-fatigue test phase***
  - Characterization of the fatigue- tested base material specimens and surface treated specimens by using techniques such as optical microscopy, Scanning Electron Microscopy (SEM), X-ray diffraction (XRD), etc.
  - Analysis of fatigue test data including plotting of S-N curves, Basquin curves, calculation of stress-modification as well as cycle modification factors

- Finite element analysis (FEA) of fatigue test specimens to find-out stress patterns in surface treated layers and correlate the same with observed fatigue test results
- Analysis of above parameters for various surface treatments to determine effect of these treatments on base material in terms of fatigue life

Pre-fatigue test phase

3.2 Material selection

A low-alloy steel based on grade En-24 as per BS: 970 (equivalent to AISI 4340 steel) was selected for conducting the research work. This material is widely used for shafts in rotating machines. The specification and properties of this material are given in Table 3.1 and 3.2.

Table 3.1: Material specifications of the test specimens

Parameters	**Specifications**			
Material grade	En-24 (as per BS 970-1-1983) (equivalent to AISI 4340 steel)			
Diameter of the bars supplied	20 mm (max.)			
Condition	Hot- rolled bars			
Grain size	6 max. (as per ASTM E-115)			
Max. permissible inclusion rating (i=Index, as per IS 4163 – 2004)	A-type (Sulphide)	B-type (Aluminate)	C-type (Silicate)	D-type (Oxide)
	i=1.5	i=1.5	i=1.5	i=1.0

Table 3.2: Chemical composition of the steel used as per grade En-24

Element	**Specified values as per standard, weight %**	**Observed values, weight %**
Carbon	0.35 – 0.45	0.396
Silicon	0.10 – 0.35	0.293
Manganese	0.45 – 0.70	0.629
Phosphorous	0.05 max.	0.013
Sulfur	0.05 max.	0.018
Nickel	1.30 – 1.80	1.425
Chromium	0.90 – 1.40	0.996
Molybdenum	0.20 – 0.35	0.205

The required quantity of En-24 steel was calculated based on the requirements of the Statistical Factorial Experiment Design developed. The entire material quantity

required for conducting the experimental program as indicted in the work plan below was obtained from a single melt and single piece of coil of wire-rod. This ensured uniformity in chemical composition and other properties such as grain size, level of decarburization, as well as content and distribution of non-metallic inclusions. Pre-procurement quality assurance for chemical composition, microstructure, inclusion rating, grain size, hardness, etc, as per the relevant test specifications was rigorously conducted on a sample basis. The final material was obtained after sequential wire drawing in the form of scale and decarburization- free rods of 18.7 mm diameter.

3.3 Specimen design and fabrication

The test specimens were prepared from 18.7 mm dia. AISI 4340 steel wire rods by machining to grip diameter of 17 mm and gauge diameter of 12 mm containing a semi-circular notch of depth 1.5 mm and root radius of 1 mm. This design of specimen results into a stress concentration factor of 2 (at notch root), as computed using analytical elastic stress analysis formulae. Figure 3.1(a) and (b) show the schematic and the detailed engineering drawing of the test specimen with dimensions duly marked over it. Further, to predict the true stress state at the notch root in the specimen under various loads applied as per the test, matrix explicit elastic-plastic FEM analysis has also been conducted for validation. This specimen design has been chosen to ensure that all the chosen alternating stress levels as per the DOE are easily spanned in the experimental program and the out-of-plane displacement of the sample at the highest applied load is kept well-within the mandated limits required for accurate fatigue testing.

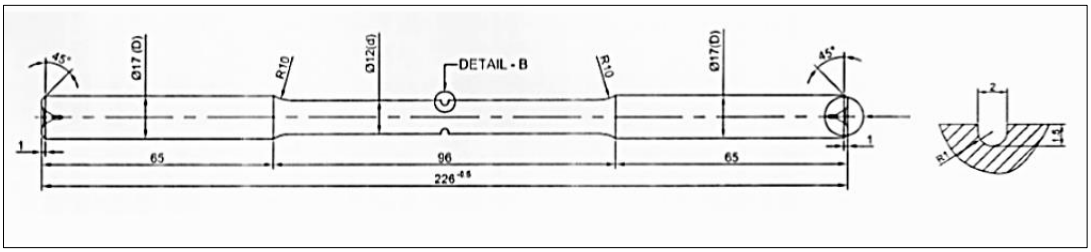

Fig. 3.1 (a): Schematic of the fatigue test specimen

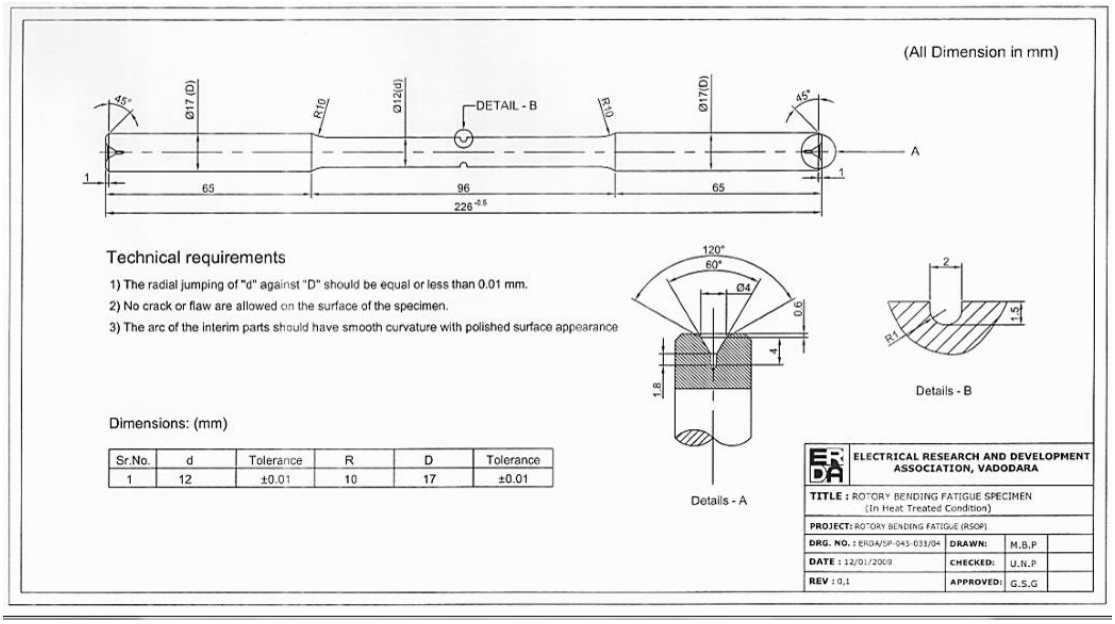

Fig. 3.1(b): Engineering drawing of the fatigue test specimen

Before carrying out the surface modification treatments on these specimens, they were subjected to hardening and tempering. Initially, preheating of the specimens was done to control distortion of specimen due to thermal stresses as eccentricity of maximum 10 microns can be allowed for the fatigue machines.The specimens were preheated at a temperature of 500 ^{0}C, followed by austenitizing at 850-860 ^{0}C for hardening and quenching in oil. The as-hardened specimens were subsequently tempered at 520 ^{0}C ± 10 ^{0}C to obtain a hardness of 32±2 HRc. Table 3.3 gives the summary of the heat treatment parameters at a glance.

Table 3.3: Heat treatment parameters at a glance

Parameters	Details
Preheating at temperature	500˚C
Hardening temperature	850˚C to 860˚C
Soaking time	12 minutes
Quenching medium	Oil
As-quenched hardness	45 to 52 HRC
Tempering temperature	520˚C ± 10˚C
Tempering time	1.5 hours
Hardness after tempering	32±2 HRC

The mechanical properties of the heat treated specimens are given in Table 3.4.

Table 3.4: Mechanical properties of the base material after heat treatment

Parameter	Observed values
Yield Strength σ_y, (MPa)	1073
Ultimate Tensile strength σ_u, (MPa)	1142
% Elongation, δ	13
% reduction in area, ΔA	44
Hardness, Rc	32±2

3.4 Surface treatments

3.4.1 Hard chrome plating

Pre-treatment surface cleaning of specimen was done by acid pickling (in 30% hydrochloric acid solution give composition) at 55 °C for 30 min for complete removal of scale followed by degreasing in acetone for 15 min. The degreased specimens were subjected to hard-chrome plating using an electro-chemical process. Chromic acid solution was used for plating. Process was carried out at 55 °C. Process parameters (current and time) were set by carrying out chrome plating of dummy samples initially and taking thickness measurements on them. The chrome-plated specimens were subjected to a baking treatment in an oven at 150 ^{0}C for 60 min for removal of hydrogen diffused, if any, to avoid hydrogen embrittlement. Figure 3.2 below gives the pictorial view of a typical hard chrome plated specimen.

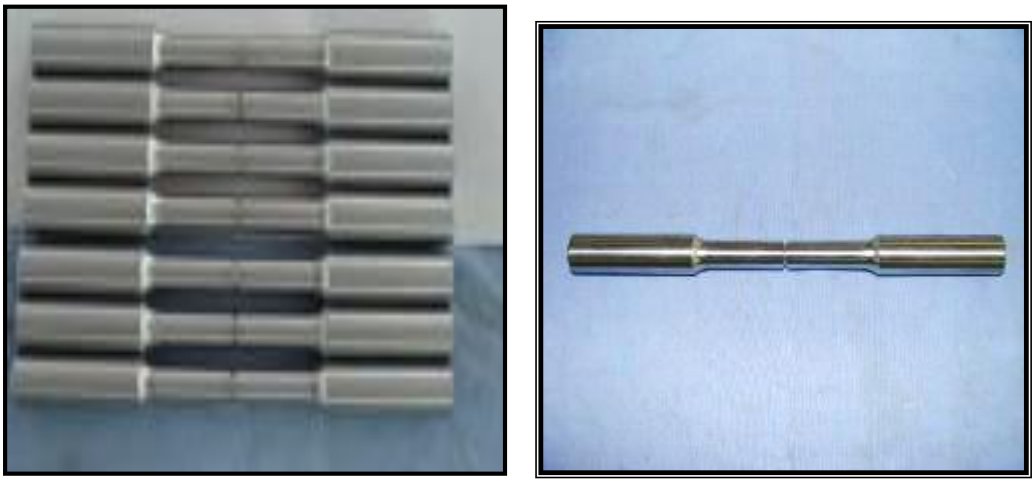

Fig. 3.2: Pictorial views of a typical hard chrome plated specimen

3.4.2Thermal spray coating of alumina powder

Thermal spraying of alumina powder was done using a flame-spray gun. An oxy-acetylene flame was used as a heating source. A bond-coat of a nickel- base alloy of approximately 150 microns was applied to ensure proper bonding of alumina coat. Alumina powder of about microns 475 - 525 µm particle size was fed into the flame through a container mounted on the gun itself. The specimen was gripped at two ends in a fixture and rotated at 100 RPM. At the same time, the flame was directed over the specimen surface and moved over its length to ensure uniform application of coat all over the surface. It was ensured that the temperature rise of specimen (during spraying) did not exceed 150 ^{0}C. Process parameters (fuel gas flow, time & feed rate of powders) were set by conducting coating of dummy samples initially and taking thickness measurements on the same. A close-up view of alumina coated specimen produced by thermal spraying is given in Fig. 3.3 below. Figure 3.4 shows the pictorial view of the thermal spray set-up used for coating alumina.

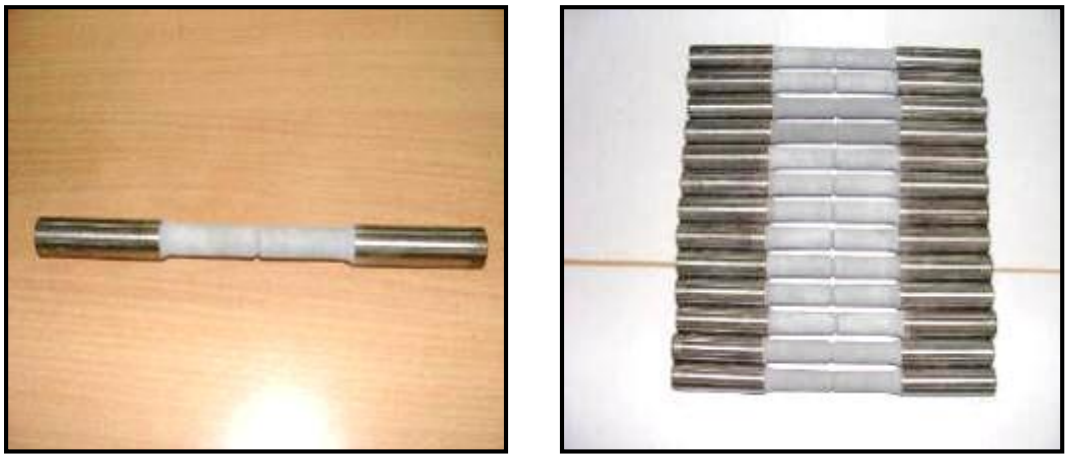

Fig. 3.3: Close-up views of alumina coated specimens produced by thermal spraying

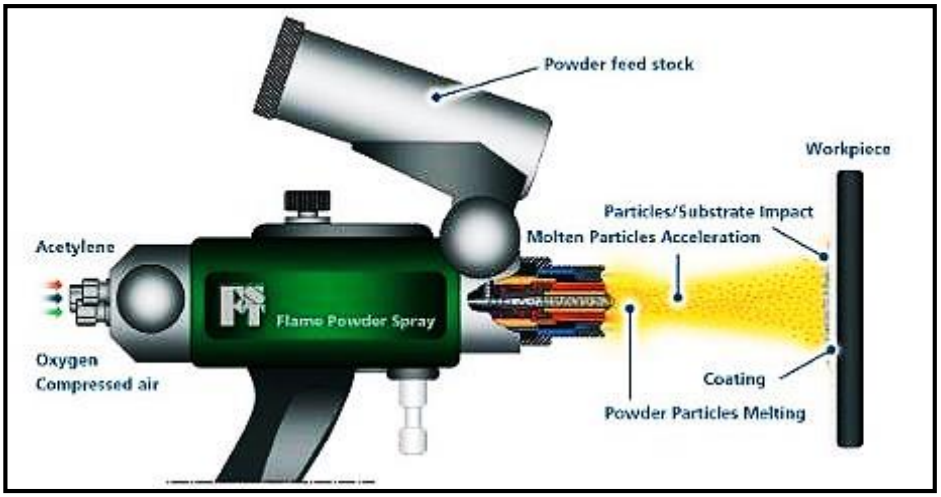

Figure 3.4: Pictorial view of the thermal spray set-up used for coating alumina

(Courtesy: Flame Spray Technologies BV, Netherlands)

3.4.3 Plasma nitriding

In plasma nitriding, the chemistry of the surface can be controlled by controlling the process parameters at three different levels of process control sophistication. The more sophisticated process control, which is also "commercially more expensive", results in controlled generation of α (interstitial nitrogen containing ferrite with carbonitrides) + γ' (FCC interstitial compound phase corresponding to stoichiometry Fe_4N). This surface microstructure typically results in generation of second and third order residual compressive surface stresses of as high as 200 MPa. On the other end, the lowest level of process control, in addition to leading to formation of an inner α and α+γ' microstructure, also results in formation of a surface microstructure called as compound layer / white layer of greater than 10 μm thickness of pure γ' (FCC interstitial compound phase corresponding to stoichiometry Fe_4N) or γ'+ε (HCP phase with stoichiometry Fe_3C) or even pure ε. While these surface chemistries can give outstanding corrosion resistance; the spalling and galling resistance tends to be dramatically degraded. Compared to these two situations, the intermediate level of process control results in the formation of a surface microstructure of less than 10 μm thick white layer of pure γ'(FCC interstitial compound phase corresponding to stoichiometry Fe_4N) or γ'+ ε (HCP phase with stoichiometry Fe_3C). In the present investigation, microstructures corresponding to these three process control regimes of plasma nitriding have been investigated for their fatigue properties. Hence, processing conditions of plasma nitriding were selected in such a way so as to get plasma nitrided

specimens (i) without white layer, (ii) with white layer less than 10 μm, and (iii) with white layer greater than 10 μm.

To achieve this, plasma nitriding of heat treated specimens was carried out in a 500 mm dia. x 500 mm height bell- shaped stainless steel vacuum chamber. The specimens were mounted on the sample holder and the chamber was evacuated to a base pressure of 0.05 mbar. The specimens were first sputter cleaned using N_2–H_2 gas mixture having 25% : 75% ratio and the pressure was raised to 1 mbar. Plasma was generated using a D.C. pulsed power supply of 800 V, 10 A, 30 kHz frequency rating. After completing the sputter cleaning process, the mixture of nitrogen and hydrogen gas was introduced into the chamber. Plasma nitriding was carried out to obtain three different categories of specimens with respect to compound layer thickness. The respective categories so developed are: specimens without any compound layer, specimens with less than 10 micron thickness of the compound layer and the specimens with more than 10 micron thickness of compound layer, respectively.

In order to obtain variation in thickness of compound layer with similar diffusion zone, plasma nitriding was carried out in two batches with different operating parameters. While, the plasma nitriding temperature (560 ^{0}C), time (24 hrs) and gas pressure (4.6 mbar) were kept constant for both the batches, the composition of nitriding gas mixture was varied. The gas mixture compositions used were in the ratio of 80:20 and 65:35 of H_2 & N_2 gas, respectively. Accordingly, for higher nitrogen content (35 % vol) of $65H_2$:$35N_2$ gas mixture, the compound layer thickness increased up to 20 micron, while it was 10 micron for lower nitrogen content (20 % vol) in a gas mixture of $80H_2$:$20N_2$. Half of the total number of specimens from the lot of 10 micron thickness were subjected to grinding to remove compound layer so as to have specimens without any compound layer. Figure 3.5 and 3.6 give the pictorial views of a plasma nitrided specimen and the set-up used, respectively.

Fig. 3.5: Pictorial view of a plasma nitrided specimens

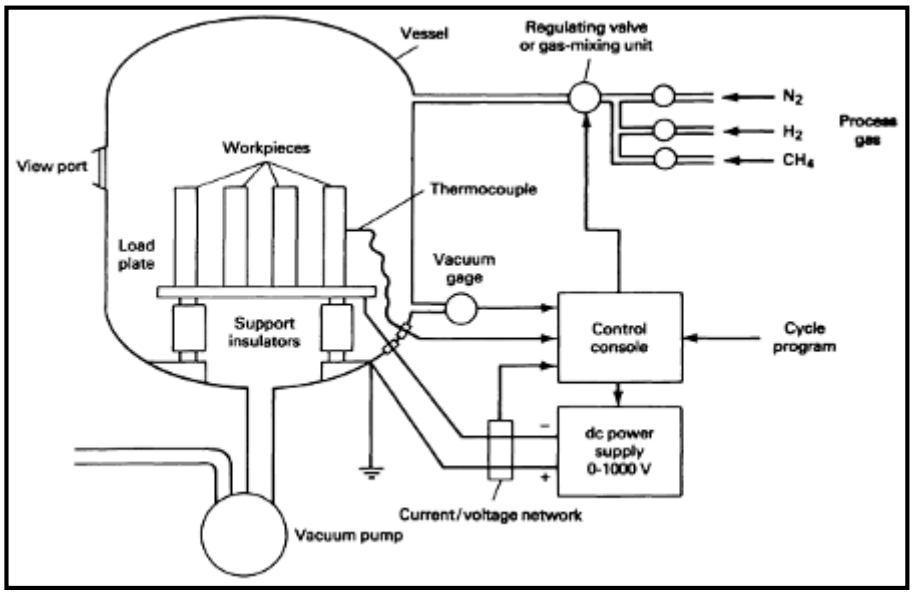

Fig. 3.6(a): Schematic of Plasma nitriding process

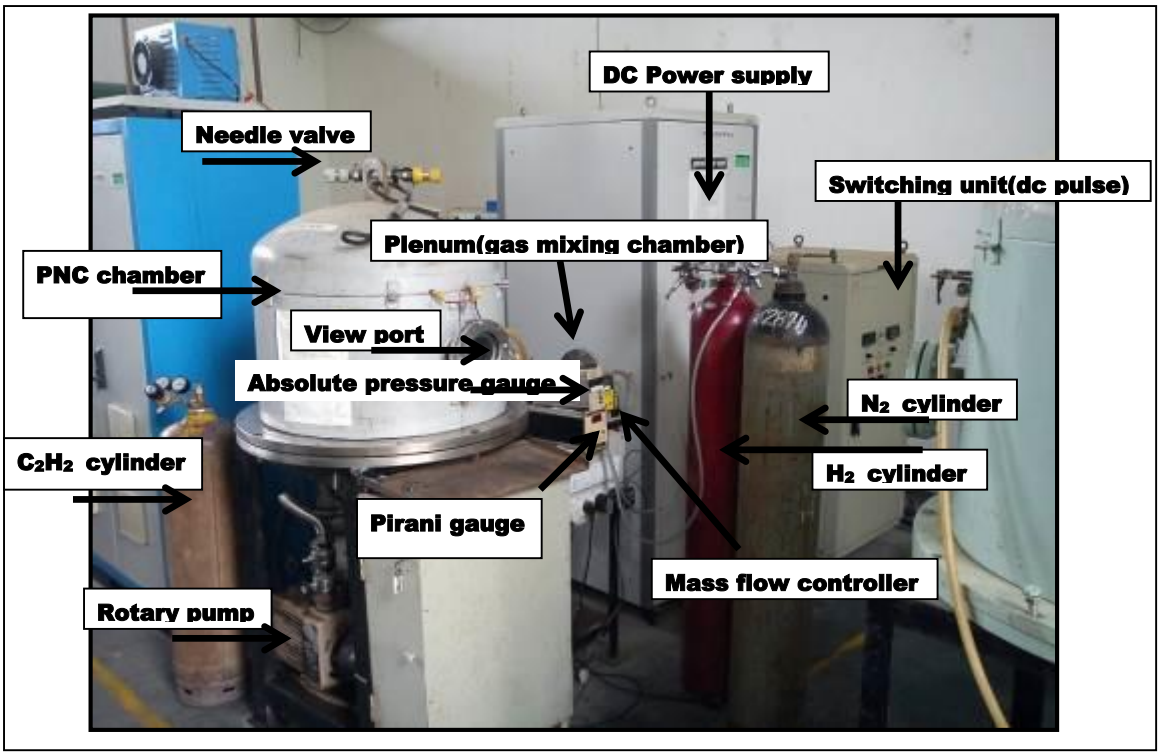

Fig. 3.6(b): Pictorial view of the plasma nitriding set-up

The different components of the Plasma nitriding system are as under:

- The stainless steel (acting as anode) chamber, in which the plasma was produced.
- A rotary pump used to create vacuum inside the vessel.
- Pirani gauge to measure the pressure of the gas inside the vessel.
- An absolute gauge used to measure the pressure at higher range than the pirani gauge.
- A heater (2kW rating) used to heat the sample and connected to a variac (230 V – 30 A) used to reach the process temperature. J-type thermocouple was used to measure the temperature of the sample.
- A high voltage DC power supply having a rating of 800 V, 10 A, 30 kHz frequency used to provide voltage to the electrodes.
- A switching unit DC pulse used to convert DC into DC pulse.
- A view port provided to view the plasma process.
- Hydrogen cylinder.
- Nitrogen cylinder.
- Acetylene cylinder.

Step-wise procedure followed for plasma nitriding is as under:

i. The samples were placed in the chamber.
ii. Vacuum to a base pressure of 10^{-3} mbar was generated in the chamber using a rotary pump.
iii. Once the desired pressure was achieved the heater was switched on, which is connected to a variac.
iv. Further plasma was created using a power supply having a rating of -800 V, 10 A, 30 kHz frequency using DC power supply.
v. Sputter cleaning of samples was carried out for 1 hour at 250 ºC using hydrogen gas to maintain a pressure of 1mbar.
vi. After sputtering, flow of hydrogen gas was decreased and simultaneously nitrogen and acetylene gases were purged in the required ratio to maintain a pressure of 5 mbar.
vii. After the required treatment- temperature is obtained the nitriding process was carried out for desired time period.
viii. After the completion of process, voltage was decreased and the flow of hydrogen gas was stopped, only nitrogen gas was allowed to flow during cooling, till 180 ºC temperature is achieved.
ix Finally after cooling, chamber was vented and the samples were taken out of the chamber.

Fatigue testing phase

3.5 Fatigue testing

3.5.1 Fatigue test method and equipment details

In the present work, smooth bar rotating bending fatigue testing approach, using a R. R. Moore type rotating bending fatigue testing machine has been adopted. Essentially, the specimen is supported as a four point (pin hinged) beam. Two of the support points are the points of load application, while the remaining two points are reaction support points. When the specimen is rotated, the bending moment generated by the four points loading results in the creation of an alternating, fully- reversed, compression-tension stressing of fibers located away from the neutral axis of the specimen. Four concurrently run fatigue testing machines were used for conducting the experiments. Details of the fatigue machines used for conducting fatigue tests are given in Table 3.5 below whereas Fig. 3.7 to 3.9 show the pictorial views of the machine:

Table 3.5: Specifications of rotary bending fatigue testing machine used

Parameters	Details
Manufacturer	Jinan TE Corporation, China
Model	PQ-6
Specimen diameter	12 mm & 17 mm
Length of the specimen	226 mm
Max. bending moment applied	60 N.m
Speed	3000 RPM (approx.)
Counter capacity	1×10^7
Motor rating	380V, 0.8kW, 3000RPM

Fig. 3.7: Pictorial view of the rotating bending fatigue machine
(*Numbers of machines installed* : 4)

Fig.3.8: Close-up view of fatigue testing machine showing loading system, controller and digital counter

Fig.3.9: Close- up view showing specimen mounted on machine

3.5.2 Methodology for fatigue testing

To generate sufficient data for analysis, minimum of four number of fatigue test specimens were subjected to each of the stress level. In all, six stress levels were used for plotting of S-N curves for each category of test specimens. Table 3.6 gives the details of tests performed on various fatigue test specimens as per statistical design of experiments.

Table 3.6: Design of Experiments as per statistical guidelines

Specimen details	Total number of tests
Specimens without surface treatment	24 (4 replicates x 6 stress levels)
Hard chrome plated specimens	24 (4 replicates x 6 stress levels)
Specimens thermally spray with alumina	24 (4 replicates x 6 stress levels)
Plasma nitrided specimens	24 (4 replicates x 6 stress levels)

3.5.3 Stress versus life cycle data

The data generated as per aforesaid fatigue testing program was plotted as S-N curves i.e. stress versus number of reversals of stress cycles. From the fatigue test data obtained, extracted mean field parameters were determined using the Basquin relationship as under:

$$\sigma_a = \alpha\left(N_f\right)^{\beta} \quad \text{----------} \qquad (3.1)$$

Where:

σ_a = alternating stress (stress amplitude)

N_f = Number of cycles to failure

α , β = Basquin pre-exponent and fatigue life exponent, respectively

Once the Basquin type relationship given by Equation 3.1 has been developed for the base material and various treatment categories, the following additional parameters are extracted for deriving the effect of "surface modification" on the fatigue life/strength. The two fatigue modification factors evaluated during this study are Fatigue stress modification factor, $(\theta_{coat})_i$ and the Cycle modification factor, Ψ_i .

These factors indicate the effect of surface treatment on the fatigue life of base the material. The effect on fatigue life can be derived with respect to change in applied stresses on the component for a particular life cycle or the total number of cycles for a particular stress being applied. The value of above mentioned factors indicates enhancement or reduction in fatigue life. The value of factor being equal to '1' means no effect on fatigue life, i.e. neither increase nor reduction in fatigue life. Value of factor >1 indicates enhancement in fatigue strength whereas < 1 indicates reduction in fatigue strength. The formulae used for calculations of these factors are given below:

3.5.3.1 Fatigue stress modification factor, $(\theta_{coat})_i$

$$(\theta_{\text{coat}})_i = \frac{(\sigma_a)_i}{(\sigma_a)_b} = \frac{\alpha_i (N_f)^{\beta_i}}{\alpha_b (N_f)^{\beta_b}} = \left[\frac{\alpha_i}{\alpha_b}\right]\left[N_f^{(\beta_i - \beta_b)}\right] = \theta_{PEi} N_f^{\theta_{Ei}} \quad \text{-------- (3.2)}$$

Where:

i = i^{th} treatment category

b = Base material

α_i , α_b = Basquin pre-exponent for i^{th} treatment and base material categories, respectively

β_i, β_b = Basquin exponent for i^{th} treatment and base material categories, respectively

θ_{PEi}, θ_{Ei} = Life reduction pre-exponent and exponent, respectively for treatment i.

3.5.3.2 Cycle modification factor, Ψ_i

$$\frac{(N_f)_i}{(N_f)_b} = \Psi_i = \frac{\xi_i (\sigma_a)^{n_i}}{\xi_b (\sigma_a)^{n_b}} = \left[\frac{\xi_i}{\xi_b}\right]\left[\sigma_a^{(n_i - n_b)}\right] = \Psi_{PEi} \sigma_a^{\Psi_{Ei}} \quad \text{---------- (3.3)}$$

Where:

i = i^{th} treatment category

b = base material category

ξ_b, ξ_i = Inverse Basquin pre-exponent for base material and i^{th} categories, respectively

η_b, η_i = Inverse Basquin Exponents for base material and i^{th} categories, respectively

Ψ_{PEi}, Ψ_{Ei} = Cycle reduction pre-exponent and exponent, respectively for i^{th} treatment.

Post-fatigue test phase

3.6 Post-surface treatment characterization

3.6.1 Coating thickness measurement:

Coating thickness of the specimens of three different surface treatments was measured microscopically on the transverse sections of the specimens that were not subjected to fatigue testing. Measurements were made in un-etched condition for hard-chrome and thermally sprayed specimens and for those of plasma nitriding treatment were made in etched condition. The coated specimens were cut in transverse plane and mounted using hot-moulding compound (bakellite) to retain the surface layer during subsequent polishing on abrasive papers. Metalllographic sample preparation technique was adopted for polishing and etching. Hard chrome plated and thermal sprayed specimens were checked for surface layers in as-polished condition. Nitrided specimens were etched using 4% nital solution. Hard-chrome plated as well as thermal sprayed specimens were observed under optical microscope at magnifications of 100x, while nitrided specimens were observed at 1000x for coating thickness measurement.

3.6.2 Surface hardness measurement:

Surface hardness of the specimens was measured using an ultrasonic hardness tester, Model MIC 20 of GE make. The machine works on principle of UCI (Ultrasonic Contact Impedance). The probe is kept on the specimen and pressed evenly against the surface. The pressure is increased steadily until the probe's specific load is attained and an acoustic signal is clearly audible. The measured hardness value is displayed on the screen. At least three readings were taken for each specimen and the statistical average has been reported.

3.6.3 Surface roughness (R_a) measurement:

Surface roughness of the specimens subjected to different surface treatments was measured in R_a units using Surface Roughness meter of Mittutoyo make model 178-602.

For this measurement, probe (stylus) of meter was moved on a length of 5 mm on surface of the specimen. An average value of roughness displayed on the meter was noted. For each specimen, readings were taken at ten locations to cover the whole specimen surface and a statistical average was found out.

3.6.4 Microhardness profile determination:

Plasma nitrided specimens were also subjected to determination of micro-hardness profile using a microhardness tester (Model LM-300 AT of Leco, USA make) at a load of 100g. The total case depth of nitriding was estimated using this data. Hardness value of 400 Hv was taken as the threshold core-hardness.

3.6.5 EDS analysis:

Composition of the layers obtained using different surface treatments was qualitatively analysed using Energy Dispersive Spectroscopy (EDS) attachment of Oxford, USA model INCA X-sight coupled to the Jeol make SEM Model JSM 6380 LV.

EDS method was also used to determine the nitrogen profile in the diffusion layer i.e. variation of nitrogen concentration in diffusion layer from surface to core for three different categories of specimens viz. plasma- nitrided with less than 10 microns white layer thickness, plasma- nitrided with more than 10 microns white layer thickness and plasma- nitrided but without any white layer.

3.6.6 Macrofractography:

The fracture surface of fatigue tested specimens was examined under stereo microscope (Olympus, Japan, make model SZ 61) from macrofractography view point. The study involved the identification of nature of fracture as regards the high-stress low-cycle or low-stress high cycle fatigue, number of crack origins & their location and overall assessment of the fracture surface. The fractographic examination of the fractured surface of the fatigue tested specimens was done at magnifications ranging from 5x to 100x.

3.6.7 Microfractography:

The fracture surface of fatigue tested specimens was also subjected to SEM fractography using Scanning Electron Microscope (SEM), Jeol, Japan make model JSM 6380 LV at various magnification ranging from 25x to 2000x. The purpose of microfractography using SEM was to examine the nature of the surface layers developed, their bonding with the substrate i.e. base material, nature and location of fatigue cracks developed, estimation of fatigue zone and fast fracture zone on the fracture surface.

3.6.8 Microstructural examination:

The microstructural examination was carried out on untreated as well as surface treated metallographic specimens. The mounted specimens were examined under optical microscope at magnifications ranging from 100x to 500x. Hard chrome plated and thermal sprayed specimens were examined in as-polished condition whereas plasma nitrided specimens were examined after etching with 4% nital solution.

3.6.9 XRD analysis:

The X-ray diffraction method was used for the determination of phases present in various surface treated specimens. The diffraction profiles were obtained using Bruker make D8 Advance X-ray diffractometer within the 2θ range of 35^0 - 90^0 at a scan step time of 8.255 sec using Cu target and Cu- Kα radiation of 0.154056 nm wavelength at a power rating of 45 kV and 40 mA. For plasma nitrided specimens emphasis was laid on determination of presence or absence of the γ-Fe_4N and ε-$Fe_{2,3}N$ phases in compound layer. Specially designed test coupons were used for this purpose.

3.7 Finite element analysis (FEA):

To rationalize the key finding of this study, namely that white layer thickness below 10 µm does not degrade the fatigue life while white layer thickness of greater than 10 µm results in reduction in fatigue life to below the threshold fatigue life of the base material, it is pertinent to note that X-ray diffraction analysis clearly indicates that the constitution of the white layer for thickness below 10 µm is predominantly Fe_4N while for thickness greater than 10 µm it is $Fe_{2-3}N$. Since the elastic constants of the $Fe_{2-3}N$ and Fe_4N are significantly different, it is reasonable to conjecture that the magnitude of the state of stress in white layers with predominant $Fe_{2-3}N$ and Fe_4N phase constitution, respectively may be significantly different in comparison to the base material under identical external loading conditions. Demonstration of existence of such differences in the state of stress in the two types of white layers will then open-up possibility of direct correlation of the stress state in the white layer with the observed behavior of the fatigue life as a function of thickness of the white layer.

For this purpose, recourse was taken to static elastic stress analysis in the isotropic solid approximation. This analysis was conducted in the following sequence:

i. Explicit 3D model of a reduced section of the fatigue specimen using Solid Works package.
ii. Formulation and solution of a closed form analytical solid mechanics model of the "Composite beam" fatigue specimen using a tractable geometrical approximation for the purpose of validation of the FEM results.
iii. Meshing of the Solid Works generated 3D model after importing into FEM based structural analysis package of ANSYS.
iv. Stress state solution using steady state elastic analysis.
v. Comparison of results with the closed form solution obtained in step ii, above for the purpose of validation of the FEM analysis.
vi. Tuning of the FEM model and determination of stress state as a function of white layer thickness for white layers of Fe_4N & $Fe_{2-3}N$ constitution.

FEM software version 14 & 15 of ANSYS was used for modelling, meshing, as well as stress analysis. A 3D CAD model of the specimen was prepared. Finite Element Meshing of the specimen was done to generate elements. Properties were assigned to materials including base material and coatings. Boundary conditions were applied on the specimen for load & displacement (constraints). Output parameters (plots) in terms of stresses generated (Max. normal stresses) were obtained. The stress values were correlated with behavior observed during fatigue testing.

The basis of the Finite Element Method used is presented in Annexure-III and details of the work carried out are presented in following section:

3.7.1 FEM based analysis on fatigue test specimen

A 3D solid model of the relevant portion of the fatigue specimen was developed in Solid Works package and a number of such models were replicated using various thicknesses of white layer ranging from 5 µm to 20 µm. A 3D CAD drawing of full size fatigue test specimen is shown in Fig. 3.10.

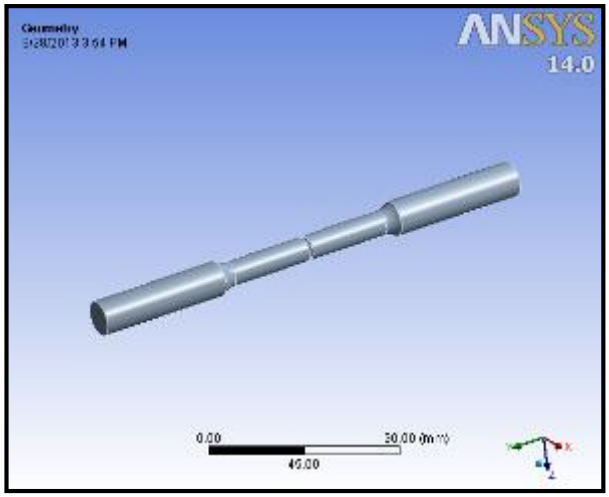

Fig. 3.10: 3- D drawing of the full size fatigue test specimen.

The following cases were considered for FEM analysis of the fatigue specimen. Stress analysis was done for a case of bending moment of 5000 Nmm.

Table 3.7: Geometry configurations considered for analysis

Case	Compound layer configuration	
	Thickness of Fe_4N Layer, µm	**Thickness of $Fe_{2-3}N$ Layer, µm**
I	5, 10, & 20	Nil
II	Nil	5, 10, & 20
III	10	5
IV	10	10

Table 3.8: Properties assigned to the base material & phases in compound layer

Material / Phase in compound layer	Properties	
	Young's modulus *E*, GPa	**Poisson's ratio *ν***
Base material	210	0.30
γ′-Fe_4N*	162	0.36
ε-$Fe_{2-3}N$ **	243	0.29

*[2.147] and ** [2.142]

The representative 3-D models, meshed model and models with boundary conditions applied are shown for each case in the Figures 3.11 to 3.13.

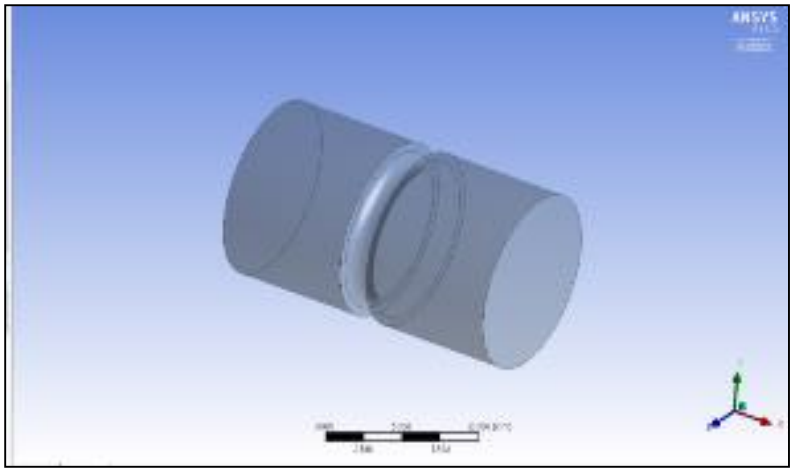

(a)

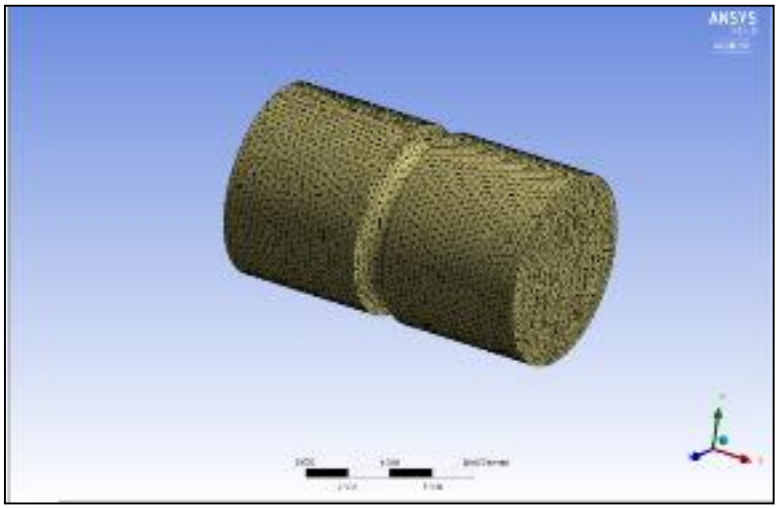

(b)

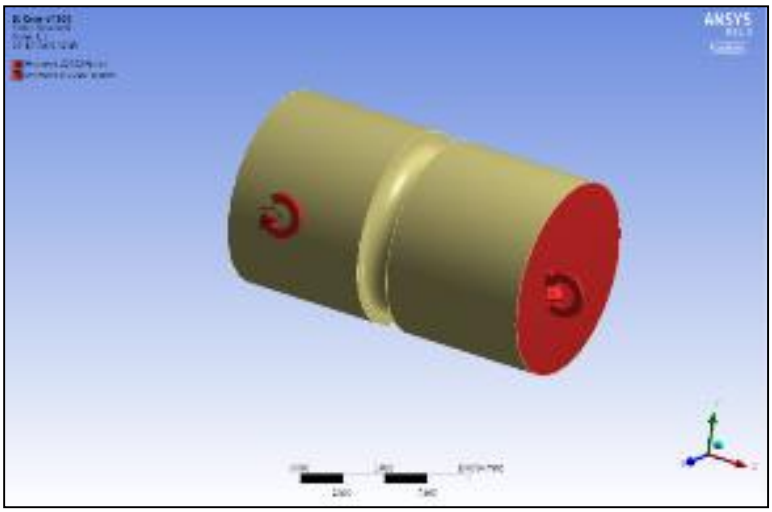

(c)

Fig. 3.11: FEM modeling for analysis of untreated specimen

(a) 3-D CAD model (b) Meshed model and (c) Model with boundary conditions

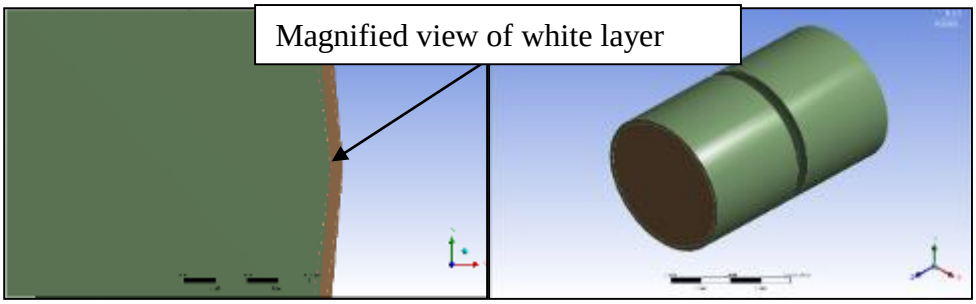

(a)

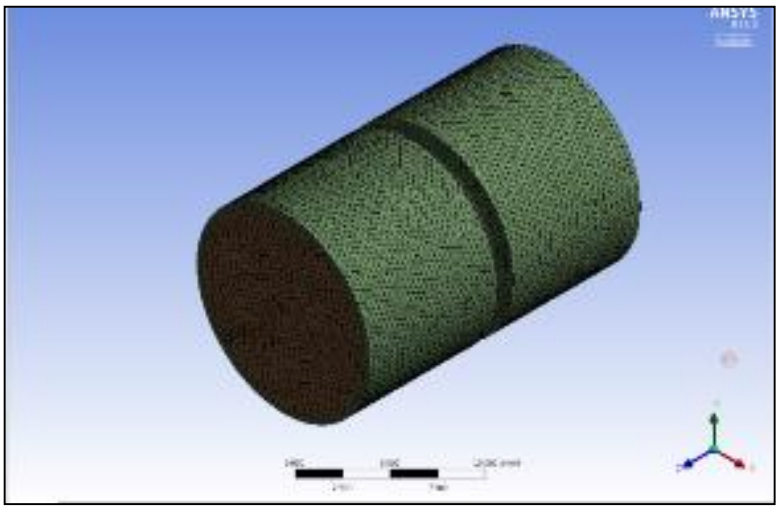

(b)

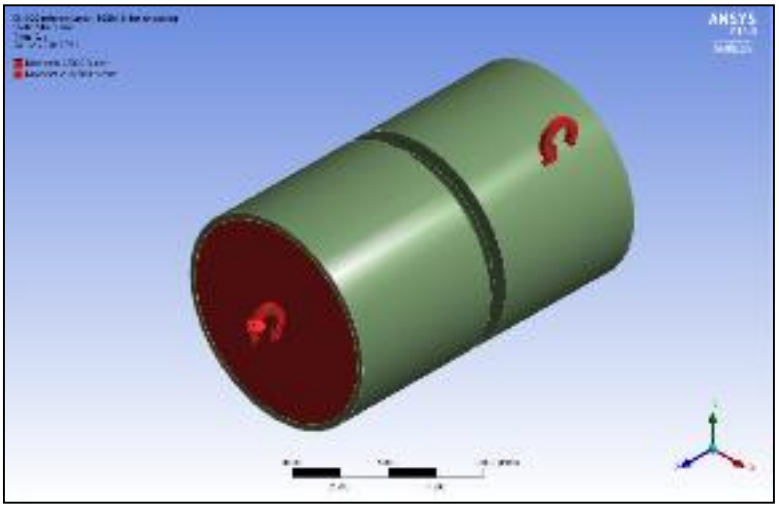

(c)

Fig. 3.12: FEM modeling for analysis of Fe_4N layer

(a) 3-D CAD model (b) Meshed model and (c) Model with boundary conditions

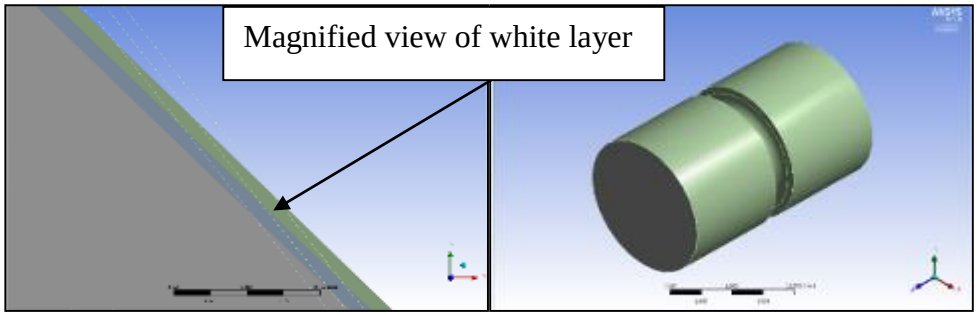

(a)

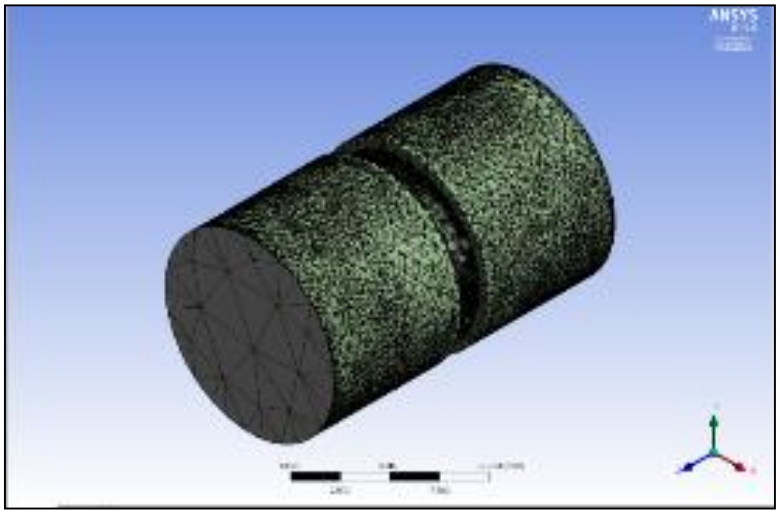

(b)

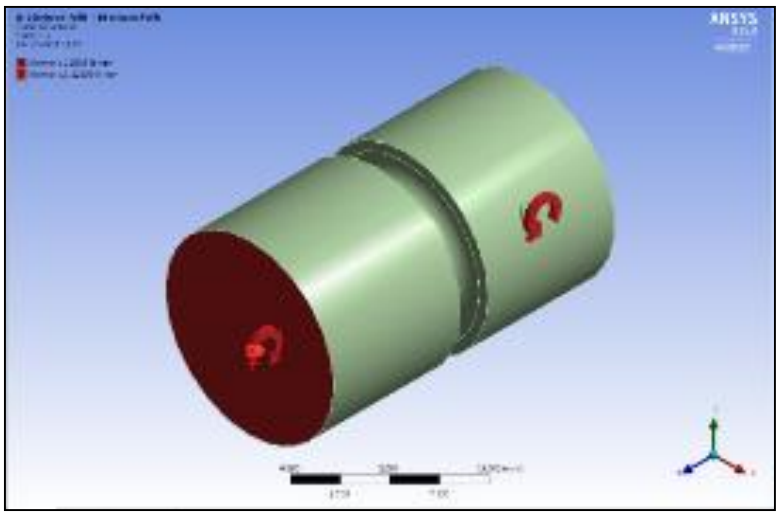

(c)

Fig. 3.13: FEM modeling for analysis of composite white layer (a) 3-D CAD model (b) Meshed model and (c) Model with boundary conditions